such as that offered in Fig. 6 provide one starting place for evaluation.

Synthesis of optically enriched biaryl compounds using enantioselective catalysts and dynamic kinetic resolution should enable improved access to stereodefined atropisomeric materials. More broadly, the approach described herein may also stimulate related research involving selective reactions of other interconverting, axially chiral compounds, promoted by simple peptide-based catalysts.

References and Notes

1. J. Kenner, W. V. A. Stubbings, *J. Chem. Soc.* **119**, 593 (1921).
2. R. Adams, H. C. Yuan, *Chem. Rev.* **12**, 261 (1933).
3. R. W. Stoughton, R. Adams, *J. Am. Chem. Soc.* **54**, 4426 (1933).
4. E. L. Eliel, S. H. Wilen, Eds., *Stereochemistry of Organic Compounds* (Wiley, New York, 1994), pp. 1142–1148.
5. D. Seebach *et al*., *Tetrahedron* **53**, 7539 (1997).
6. J. Clayden, W. J. Moran, P. J. Edwards, S. R. LaPlante, *Angew. Chem. Int. Ed.* **48**, 6398 (2009).
7. R. Noyori, H. Takaya, *Acc. Chem. Res.* **23**, 345 (1990).
8. G. Bringmann *et al*., *Angew. Chem. Int. Ed.* **44**, 5384 (2005).
9. M. Shindo, K. Koga, K. Tomioka, *J. Am. Chem. Soc.* **114**, 8732 (1992).
10. X. Li, J. B. Hewgley, C. A. Mulrooney, J. Yang, M. C. Kozlowski, *J. Org. Chem.* **68**, 5500 (2003).
11. J. Yin, S. L. Buchwald, *J. Am. Chem. Soc.* **122**, 12051 (2000).
12. T. Hayashi, K. Hayashizaki, T. Kiyoi, Y. Ito, *J. Am. Chem. Soc.* **110**, 8153 (1988).
13. G. Bringmann, D. Menche, *Acc. Chem. Res.* **34**, 615 (2001).
14. J. Clayden, S. P. Fletcher, J. J. W. McDouall, S. J. M. Rowbottom, *J. Am. Chem. Soc.* **131**, 5331 (2009).
15. F. Kakiuchi, P. Le Gendre, A. Yamada, H. Ohtaki, S. Murai, *Tetrahedron Asymmetry* **11**, 2647 (2000).
16. G. Bott, L. D. Field, S. Sternhell, *J. Am. Chem. Soc.* **102**, 5618 (1980).
17. A. I. Meyers, R. J. Himmelsbach, *J. Am. Chem. Soc.* **107**, 682 (1985).
18. S. E. Denmark, G. L. Beutner, *Angew. Chem. Int. Ed.* **47**, 1560 (2008).
19. W. Zhang, H. Xy, H. Xu, W. J. Tang, *J. Am. Chem. Soc.* **131**, 3832 (2009).
20. R. H. Mitchell, Y. H. Hai, R. V. Williams, *J. Org. Chem.* **44**, 4733 (1979).
21. S. France, A. Weatherwax, T. Lectka, *Eur. J. Org. Chem.* **2005**, 475 (2005).
22. A. Sakakura, A. Ukai, K. Ishihara, *Nature* **445**, 900 (2007).
23. S. Ahmad, D. C. Braddock, G. Hermitage, *Tetrahedron Lett.* **48**, 915 (2007).
24. S. J. Miller, *Acc. Chem. Res.* **37**, 601 (2004).
25. E. Colby Davie, S. M. Mennen, Y. Xu, S. J. Miller, *Chem. Rev.* **107**, 5759 (2007).
26. C. A. Lewis *et al*., *J. Am. Chem. Soc.* **130**, 16358 (2008).
27. T. S. Haque, J. C. Little, S. H. Gellman, *J. Am. Chem. Soc.* **118**, 6975 (1996).
28. R. Noyori, M. Tokunaga, M. Kitamura, *Bull. Chem. Soc. Jpn.* **68**, 36 (1995).
29. J. Steinreiber, K. Faber, H. Griengl, *Chem. Eur. J.* **14**, 8060 (2008).
30. Experimental procedures and compound characterization are available as supporting material on *Science* Online.
31. A. F. Littke, C. Dai, G. C. Fu, *J. Am. Chem. Soc.* **122**, 4020 (2000).
32. D. A. Watson *et al*., *Science* **325**, 1661 (2009).
33. R. Martin *et al*., *Angew. Chem. Int. Ed.* **48**, 8042 (2009).
34. A. S. Kende, L. S. Liebeskind, *J. Am. Chem. Soc.* **98**, 267 (1976).
35. F. Johnson, *Chem. Rev.* **68**, 375 (1968).

36. We are grateful to the National Institute of General Medical Sciences of the NIH for support (GM068649). Metrical parameters for the solid state structure of compound **3d** are available free of charge from the Cambridge Crystallographic Data Centre under CCDC-773872.

Supporting Online Material

www.sciencemag.org/cgi/content/full/328/5983/1251/DC1
Materials and Methods
Figs. S1 to S4
Tables S1 to S10
References and Notes

16 February 2010; accepted 21 April 2010
10.1126/science.1188403

Operation Mechanism of a Molecular Machine Revealed Using Time-Resolved Vibrational Spectroscopy

Matthijs R. Panman,[1] Pavol Bodis,[1] Daniel J. Shaw,[1] Bert H. Bakker,[1] Arthur C. Newton,[1] Euan R. Kay,[2] Albert M. Brouwer,[1]* Wybren Jan Buma,[1]* David A. Leigh,[2]* Sander Woutersen[1]*

Rotaxanes comprise macrocycles that can shuttle between docking stations along an axle. We explored the nanosecond shuttling mechanism by reversing the relative binding affinities of two stations through ultraviolet-induced transient reduction. We monitored the ensuing changes in the CO-stretching bands of the two stations and the shuttling macrocycle by means of an infrared probing pulse. Because hydrogen-bond scission and formation at the initial and final stations led to well-resolved changes in the respective CO-stretch frequencies, the departure and arrival of the macrocycle could be observed separately. We found that the shuttling involves two steps: thermally driven escape from the initial station, followed by rapid motion along the track ending either at the initial or final station. By varying the track's length, we found that the rapid motion approximates a biased one-dimensional random walk. However, surprisingly, the direction of the overall motion is opposite that of the bias.

Recent developments in the generation and control of motion on a molecular scale have enabled the construction of prototypical molecular machines (*1*–*14*). The mechanics of such molecular machines are fundamentally different from those of macroscopic machines. As a machine's size and speed approach those of the solvent molecules surrounding it, macroscopic concepts such as viscous friction lose meaning, and thermal fluctuations lead to intrinsic randomness in the machine's behavior (*15*, *16*). A detailed understanding of the motion of molecular machines requires experiments with both structural sensitivity at the atomic level and sufficient time resolution. Time-resolved vibrational spectroscopy meets both of these requirements (*17*, *18*). Probing the stretch modes of specific, localized chemical bonds affords a direct view of the conformational changes underlying the operation of individual components of the molecular machine. The time resolution of the probing is determined by the pulse duration, which can be less than 100 fs. Here, we used time-resolved vibrational pump-probe experiments on a light-triggered rotaxane shuttle to unravel its operating mechanism.

Rotaxanes consist of mechanically interlocked wheel- and axle-like components. Figure 1 shows the chemical structure of this type of molecular machine, together with its operation cycle, which we characterized previously with spectroelectrochemistry and transient ultraviolet-visible (UV-Vis) spectroscopy (*3*, *19*). In the neutral molecule, the macrocycle is hydrogen-bonded predominantly (>99%) to the succinamide station (**succ**) (*3*, *19*). After excitation of the naphthalimide station (**ni**) with a 355-nm light pulse, the rotaxane undergoes rapid (~1.6 ns) intersystem crossing to the triplet state (*20*). In this state, the **ni** station is reduced by an external electron donor to form a radical anion (**ni**$^{\bullet-}$). The **ni**$^{\bullet-}$ station has a much greater affinity for the macrocycle than does the **succ** station [equilibrium constant >1000 (*3*)]. Consequently, the macrocycle shuttles over the thread and forms hydrogen bonds to the **ni**$^{\bullet-}$ station. After slow (~100 μs) charge recombination between **ni**$^{\bullet-}$ and the radical cation of the electron donor, the macrocycle travels back over the thread and binds to the **succ** station, and the system is ready to shuttle again (*3*). In the following, rotaxanes with track length n are referred to as C_n.

The vibrational absorption spectrum of the C_{12} rotaxane in its initial state is shown in Fig. 2A. All peaks in the rotaxane spectrum can be assigned by comparison with spectra of the constituent components (*19*). The symmetric and antisymmetric CO-stretch modes of the **ni** station are observed as peaks **1** and **7**, respectively (the latter also contains a contribution from the CO-stretch vibration

[1]Van 't Hoff Institute for Molecular Sciences, University of Amsterdam, Nieuwe Achtergracht 166, 1018 WV Amsterdam, Netherlands. [2]School of Chemistry, University of Edinburgh, King's Buildings, West Mains Road, Edinburgh EH9 3JJ, UK.

*To whom correspondence should be addressed. E-mail: a.m.brouwer@uva.nl (A.M.B.); w.j.buma@uva.nl (W.J.B.); david.leigh@ed.ac.uk (D.A.L.); s.woutersen@uva.nl (S.W.)

of the macrocycle), and the CO-stretch mode of the **succ** station is observed as peak **5**.

In the time-resolved experiments, we trigger the rotaxane with a 4-ns, 355-nm pulse and observe the subsequent vibrational absorption change by means of a 100-fs mid-infrared (IR) probe pulse (*21*, *22*). In Fig. 2, B and C, we show normalized (*19*, *21*) UV-IR transient spectra of the C_{12} rotaxane at different delay times. The spectra at early delays (<120 ns) show how the triplet state evolves to the radical anion state (**ni**$^{\bullet-}$). Subsequently, the spectrum evolves further as the macrocycle shuttles from the **succ** to the **ni**$^{\bullet-}$ station (Fig. 2C). For the assignment of the peaks in Fig. 2C we use steady-state spectra of the initial, charged, and final states (*19*). Peaks **2** and **3** (labeled ARRIVAL) are the CO-stretch modes of the **ni**$^{\bullet-}$ station when it is free and when it is hydrogen-bonded to the macrocycle, respectively. The temporal evolution of these peaks therefore directly mirrors the arrival of the macrocycle at the **ni**$^{\bullet-}$ station. Similarly, peaks **4** and **5** (labeled DEPARTURE) are the CO-stretch modes of the **succ** station when free and when hydrogen-bonded to the macrocycle. The behavior of these two peaks therefore mirrors the departure of the macrocycle from the **succ** station. Peak **6** is due to the CO-stretch mode of the macrocycle when its NH groups are hydrogen-bonded to the **ni**$^{\bullet-}$ station (*19*). The corresponding absorption decrease of the CO-stretch mode of **succ**-bound macrocycles as they leave the **succ** station is superimposed on (temporally static) peak **7**.

The time evolution of the intensity of peaks **2**, **3**, **4**, **5**, and **6** is shown in Fig. 3. We find that the departure and arrival of the macrocycle can be well described with the same time constant. We performed a global least-squares fit to the data (*21*), in which the charging and shuttling are each described by a single rate constant. From the fit (see curves in Fig. 3) we obtain $k_{charge} = 2.8\ (\pm 0.4) \times 10^7\ s^{-1}$, which corresponds to the charging lifetime of 35 ± 5 ns. We find that for the C_{12} rotaxane, $k_s^{C_{12}} = 1.30(\pm 0.03) \times 10^6\ s^{-1}$; this shuttling rate constant corresponds to a shuttling time of 0.77 ± 0.02 μs, in agreement with previous UV-Vis experiments (*3*).

The fact that the departure and arrival exhibit the same dynamics implies that during the shuttling process, an individual macrocycle spends only a short time on the thread relative to the average shuttling time of the ensemble. The observed average shuttling time is therefore not determined by the time the macrocycle spends on the CH_2 chain, but rather by the time it takes for the macrocycle to escape from the initial station. The sequence of events in the shuttling of this rotaxane is thus as follows: occasional escape from the **succ** station, followed by a rapid motion over the thread, ending at either the **ni**$^{\bullet-}$ (where it can no longer escape because of the stronger hydrogen bonding) or the initial **succ** station (where it will wait until the next escape). Below, we investigate the two steps of this mechanism in more detail.

To quantify the energy barrier that the macrocycle must overcome to escape from the **succ** station, we measured the shuttling rate of a C_9 rotaxane (*23*) over a temperature range of 45 K (*21*). The temperature increase due to the partial conversion of the pump energy into heat is negligible (*21*). The temperature dependence of $k_s^{C_9}$ displays Arrhenius behavior, indicating that the escape from the **succ** station is effectively a single-barrier event and that the energy required by the macrocycle to cross it is provided by thermal fluctuations. We find that the data can be well described with the Eyring equation,

$$k_s(T) = \frac{k_B T}{h} \exp\left[-\left(\frac{\Delta G^{\ddagger}}{RT}\right)\right] \qquad (1)$$

where k_B is the Boltzmann factor, R is the gas constant, h is the Planck constant, $\Delta G^{\ddagger}$ is the Gibbs free energy of activation, and T is the absolute temperature of the system. From a least-squares fit (fig. S5), we find that the enthalpy of activation $\Delta H^{\ddagger}$ is 26 (±1) kJ mol^{-1} and the entropy of activation $\Delta S^{\ddagger}$ is −32 (±3) J mol^{-1} K^{-1}. The energy barrier $\Delta H^{\ddagger}$ is consistent with the breaking of approximately four hydrogen bonds, assuming a binding energy of −7.5 (±0.8) kJ mol^{-1} per hydrogen bond (*24*). The negative activation entropy suggests that some ordering of the system is required for escaping from the **succ** station. Folding of the thread onto itself can be excluded, as this should be evident in the **ni** and/or **ni**$^{\bullet-}$ CO-stretch response in the transient spectra (*19*). The ordering might involve a relative positioning of macrocycle and thread that is favorable for breaking the macrocycle-**succ** hydrogen bonds.

The next step in the shuttling process is the fast motion of the macrocycle over the thread, ending at either the **succ** station or the **ni**$^{\bullet-}$ station. To investigate the nature of this fast motion, we explored how changing the carbon-chain length affects the probability of the macrocycle ending at the **ni**$^{\bullet-}$ station. This probability is proportional to the observed shuttling rate, as the rate at which escape from the **succ** station occurs is independent of the carbon-chain length. The shuttling rates of rotaxanes with thread lengths n = 5, 9, 12, and 16 are shown in Fig. 4. The rate of shuttling was observed to decrease markedly with increasing thread length. We analyzed the data by modeling the motion of the macrocycle over the thread as a one-dimensional random walk. In the simplest version of this model, the C_n chain is modeled as a track of n local free-energy minima, between which the macrocycle makes random jumps, to end up at either the **ni**$^{\bullet-}$ or **succ** station. If we assume equal probabilities for the macrocycle to make one step toward

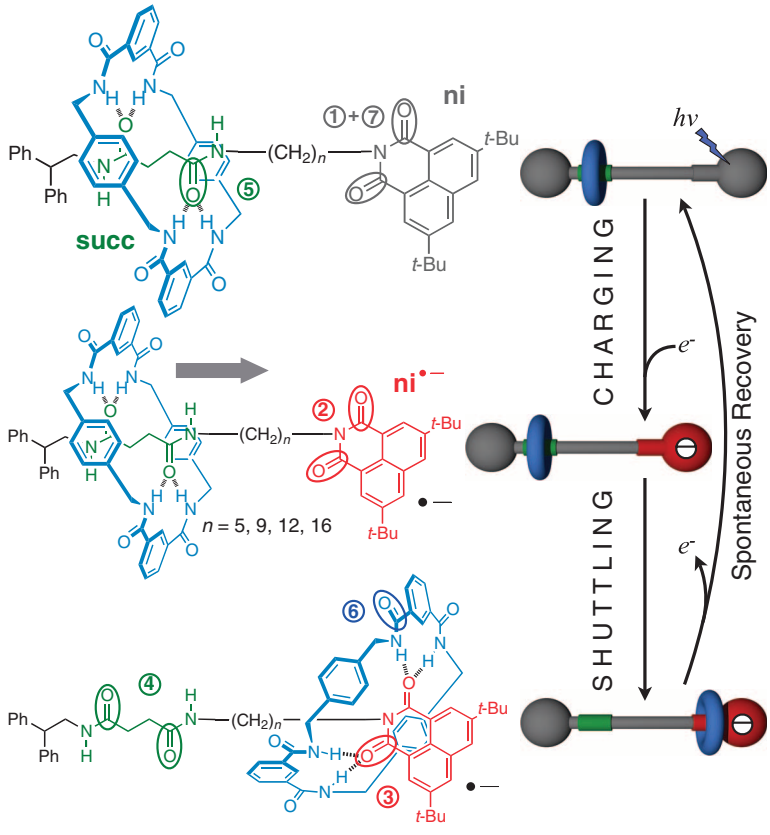

Fig. 1. Chemical structures of the [2]rotaxane shuttle in the neutral, radical anion, and shuttled radical anion states. 1,4-Diazabicyclo[2.2.2]octane (DABCO) was used as the external electron donor. We studied derivatives with different track lengths n. The labeled CO groups correspond to the labeled peaks in Fig. 2. Ph, phenyl; Bu, butyl.

either station, the probability of the macrocycle arriving at the **ni**$^{\bullet-}$ station is given by

$$P_s(n) = \frac{1}{n+1} \quad (2)$$

(*25*). A least-squares fit of the rate data to this equation, with the proportionality factor between the observed rate constant and $P_s(n)$ as the only fit parameter, is shown as the gray dashed curve in Fig. 4. Although the model reproduces the observed trend, the quantitative agreement is poor. Allowing for a certain number of CH_2 units to be occupied by the macrocycle (*25*) still results in a poor description of the data (*21*).

We find that very good agreement is obtained by introducing a small bias in the probabilities of making a step in the forward or backward direction. Assuming a probability p of hopping forward (in the direction of the **ni**$^{\bullet-}$ station), and $1 - p$ of hopping backward, the probability of arriving at the **ni**$^{\bullet-}$ station becomes

$$P_s(n) = \frac{1 - \left(\frac{1-p}{p}\right)}{1 - \left[\left(\frac{1-p}{p}\right)^{n+1}\right]} \quad (3)$$

(*26*). From a least-squares fit (with p and an overall scaling factor as the only fit parameters), we find that the best description of the data is obtained for $p = 0.442 \pm 0.003$ (red curve in Fig. 4). This value of p implies that the event of the macrocycle moving one step toward the **ni**$^{\bullet-}$ station is slightly less probable than the event of it moving toward the **succ** station ($1 - p = 0.56$); that is, the random translational motion of the macrocycle along the track has a small bias toward the **succ** station. At present, we can only speculate as to the driving force behind this bias. An enthalpic driving force seems improbable in view of the short-range nature of the hydrogen-bond interactions that give rise to the overall ΔH of the shuttling. It is more likely that the bias is mainly of entropic origin. This could be the case if the thread conformation is on average slightly more favorable to macrocycle translation at the **succ** side than at the **ni**$^{\bullet-}$ side. Interestingly, the overall motion of the macrocycle from **succ** to **ni**$^{\bullet-}$ occurs against the bias (which is toward the **succ** station). This is possible only because there is a global free-energy minimum at the **ni**$^{\bullet-}$ station.

Our findings can be summarized by combining Eqs. 1 and 3 to obtain an expression for the shuttling rate as a function of temperature and track length:

$$k_s(T,n) \propto \frac{k_B T}{h} \exp\left[-\left(\frac{\Delta G^{\ddagger}}{RT}\right)\right] P_s(n) \quad (4)$$

Each term describes one stage of the shuttling mechanism (Fig. 4, inset). The probability $P_s(n)$ for the random walk to end at the final station is <<1 [for the shortest shuttle, $P_s(5) = 0.09$; for the longest, $P_s(16) = 0.005$], so that many escapes (tens to hundreds) of the macrocycle from the initial station are required before a successful shuttling event occurs. This leads to a certain amount of randomness in the timing of the arrival of the shuttle.

A more detailed understanding of the bias against shuttling requires an exploration of the rotaxane's free-energy landscape using molecular dynamics simulations. Because shuttling is such a rare event, this will require state-of-the-art simulation methods, and we hope that our results will stimulate work in this direction. On a more fundamental level, it is noteworthy that the

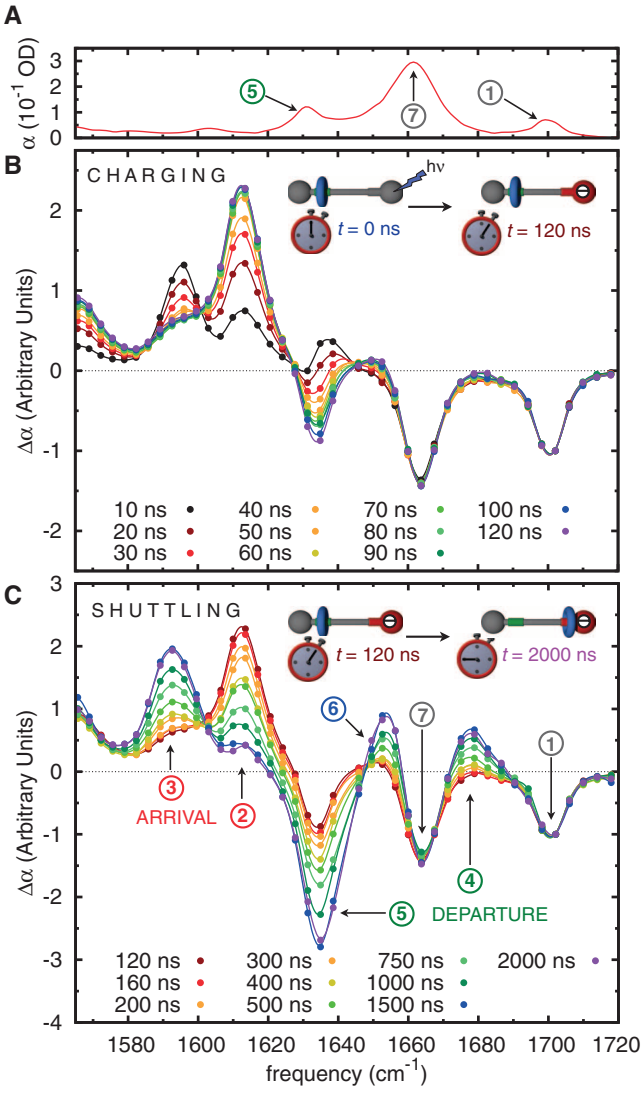

Fig. 2. (**A**) Fourier-transform IR spectrum of 10^{-4} M C_{12} rotaxane and 10^{-2} M DABCO in CD_3CN; path length 11 mm (solvent subtracted). (**B**) Transient UV-IR spectra of the C_{12} rotaxane at delays ranging from 10 to 120 ns after UV excitation. (**C**) Transient UV-IR spectra of the C_{12} rotaxane at delays ranging from 120 to 2000 ns after UV excitation. The labeled vibrations in the transient spectrum correspond to the labeled CO groups of Fig. 1.

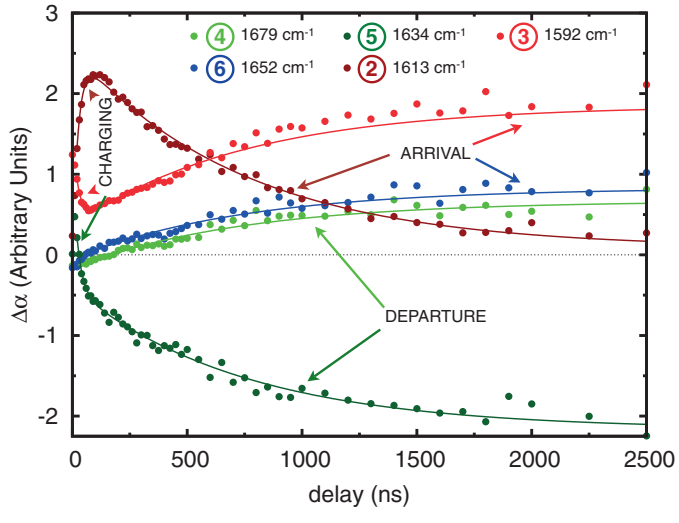

Fig. 3. Observed time dependence of the absorption peaks **2**, **3**, **4**, **5**, and **6** normalized to the maximum intensity of peak **1**, each of which corresponds to a specific CO bond in a specific state of the operation cycle; see Fig. 1. The curves represent least-squares fits of bi-exponential decays.

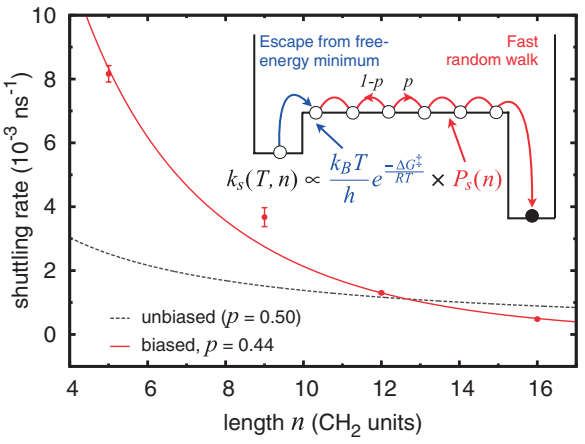

Fig. 4. Thread length (n) dependence on the shuttling rate constant k_s fitted with an unbiased random walk model and a biased random walk model (Eq. 3). The error bars represent ±1σ (*21*). The inset shows a schematic representation of the shuttling mechanism.

unpredictability of the arrival time of the shuttle does not imply unpredictability of the arrival itself. A consideration of the probability for a macrocycle to make the transition from one station to another is essentially an attempt to describe the shuttling motion—about which our experiments provide ensemble thermodynamic and kinetic information—at the single-molecule level. Fluctuation theorems (*27*) provide a connection between thermodynamic parameters and single-molecule measurements of molecular mechanical events (*28*). In particular, theoretical work on time-symmetry breaking in such measurements has shown that the free-energy change per operation cycle should be about 4 to 8 k_BT for an individual molecular machine to rectify thermal fluctuations to such an extent as to advance mostly forward in time (i.e., toward the conformation corresponding to the free-energy minimum) (*29*). The free-energy difference that drives the rotaxane's shuttling motion (the difference between the **succ**- and **ni**$^{\bullet-}$-bound macrocycle) is −18 kJ/mol (*3*), which corresponds to 7.3 k_BT. This is just enough to ensure that the shuttling occurs in the forward time direction (*29*). The rotaxane-based shuttles are thus reliable in the sense that the macrocycle will eventually arrive at the **ni**$^{\bullet-}$ station. On the other hand, our results show that with increasing length of the shuttle's track, the time at which this arrival occurs becomes more and more unpredictable.

References and Notes

1. T. R. Kelly, H. De Silva, R. A. Silva, *Nature* **401**, 150 (1999).
2. N. Koumura, R. W. J. Zijlstra, R. A. van Delden, N. Harada, B. L. Feringa, *Nature* **401**, 152 (1999).
3. A. M. Brouwer *et al.*, *Science* **291**, 2124 (2001).
4. D. A. Leigh, J. K. Y. Wong, F. Dehez, F. Zerbetto, *Nature* **424**, 174 (2003).
5. P. Thordarson, E. J. A. Bijsterveld, A. E. Rowan, R. J. M. Nolte, *Nature* **424**, 915 (2003).
6. J. D. Badjic, V. Balzani, A. Credi, S. Silvi, J. F. Stoddart, *Science* **303**, 1845 (2004).
7. J. V. Hernández, E. R. Kay, D. A. Leigh, *Science* **306**, 1532 (2004).
8. S. P. Fletcher, F. Dumur, M. M. Pollard, B. L. Feringa, *Science* **310**, 80 (2005).
9. V. Balzani *et al.*, *Proc. Natl. Acad. Sci. U.S.A.* **103**, 1178 (2006).
10. T. Muraoka, K. Kinbara, T. Aida, *Nature* **440**, 512 (2006).
11. J. E. Green *et al.*, *Nature* **445**, 414 (2007).
12. V. Serreli, C. F. Lee, E. R. Kay, D. A. Leigh, *Nature* **445**, 523 (2007).
13. S. Hiraoka, E. Okuno, T. Tanaka, M. Shiro, M. Shionoya, *J. Am. Chem. Soc.* **130**, 9089 (2008).
14. M. von Delius, E. M. Geertsema, D. A. Leigh, *Nat. Chem.* **2**, 96 (2010).
15. R. D. Astumian, *Proc. Natl. Acad. Sci. U.S.A.* **102**, 1843 (2005).
16. R. D. Astumian, *Proc. Natl. Acad. Sci. U.S.A.* **104**, 19715 (2007).
17. A. Stolow, D. M. Jonas, *Science* **305**, 1575 (2004).
18. C. Kolano, J. Helbing, M. Kozinski, W. Sander, P. Hamm, *Nature* **444**, 469 (2006).
19. D. C. Jagesar, F. Hartl, W. J. Buma, A. M. Brouwer, *Chem. Eur. J.* **14**, 1935 (2008).
20. D. C. Jagesar *et al.*, *Adv. Funct. Mater.* **19**, 3440 (2009).
21. See supporting material on *Science* Online.
22. The time resolution of the experiment is determined by the pump pulse, which is 4 ns. The 100-fs probe pulse provides us with the spectral bandwidth necessary to probe the entire rotaxane absorption spectrum in one laser pulse.
23. We chose the C_9 rotaxane for the temperature studies because of its superior solubility in CD_3CN and therefore its better signal-to-noise ratio relative to the C_{12} rotaxane.
24. M. Akiyama, T. Ohtani, *Spectrochim. Acta A* **50**, 317 (1994).
25. A. B. C. Deutman *et al.*, *Science* **322**, 1668 (2008).
26. G. Grimmett, D. Welsh, *Probability: An Introduction* (Oxford Univ. Press, Oxford, 1986).
27. C. Jarzynski, *Phys. Rev. E* **73**, 046105 (2006).
28. D. Collin *et al.*, *Nature* **437**, 231 (2005).
29. E. H. Feng, G. E. Crooks, *Phys. Rev. Lett.* **101**, 090602 (2008).

30. We thank P. Reinders, S. Kettelarij, D. Bebelaar, M. Groeneveld, H. Luiten, H. Beukers, and C. van den Biggelaar for technical support, and G. Rothenberg for valuable discussions. Supported by the European Community (EMMMA IHP Research Training Network, contract HPRN-CT- 2002-00168, and Hy3M STREP, contract NMP4-CT-2004-013525) and by the Stichting voor Fundamenteel Onderzoek der Materie (FOM), which is financially supported by the Nederlandse Organisatie voor Wetenschappelijk Onderzoek (NWO).

Supporting Online Material

www.sciencemag.org/cgi/content/full/328/5983/1255/DC1
Materials and Methods
Figs. S1 to S7
References

4 February 2010; accepted 19 April 2010
10.1126/science.1187967

The Thermodynamics of the Elusive HO_3 Radical

Sébastien D. Le Picard,[1]* Meryem Tizniti,[1] André Canosa,[1] Ian R. Sims,[1]* Ian W. M. Smith[2]*

The role of HO_3 as a temporary reservoir of atmospheric OH radicals remains an open question largely because of the considerable uncertainty in the value of the dissociation energy of the HO–O_2 bond (D_0) or, equivalently, the standard enthalpy of formation of HO_3 ($\Delta_f H^{\circ}$). Using a supersonic flow apparatus, we have observed by means of laser-induced fluorescence the decay of OH radicals in the presence of O_2 at temperatures between 55.7 and 110.8 kelvin (K). Between 87.4 and 99.8 K, the OH concentration approached a nonzero value at long times, allowing equilibrium constants for the reaction with O_2 to be calculated. Using expressions for the equilibrium constant from classical and statistical thermodynamics, and values of partition functions and standard entropies calculated from spectroscopic data, we derived values of D_0 = (12.3 ± 0.3) kilojoules per mole and $\Delta_f H^{\circ}$ (298 K) = (19.3 ± 0.5) kilojoules per mole. The atmospheric implications of HO_3 formation are therefore very slight.

The weakly bound HO_3 radical has been postulated as a transient intermediate in three processes of importance in the Earth's atmosphere (Scheme 1, reactions R1 to R3). Sridharan *et al.* (*1*) showed that when ^{18}O was used as the atomic reactant in the rapid reaction R1 with HO_2, the hydroxyl product was exclusively ^{16}OH, suggesting that the reaction occurred not through H-atom abstraction but rather via transient formation of $H^{16}O^{16}O^{18}O$. Vibrationally excited OH formed in reaction R2 is the source of the Meinel bands emitted from the upper atmosphere (*2*). The reaction leads to high yields of the OH product in the highest energetically accessible vibrational levels v = 7 to 9 (*3*, *4*), indicating energy release on a highly attractive potential energy surface (*5*), which would be the form expected if HO_3 is weakly bound relative to OH + O_2 (*4*). A third process—R3, the relaxation

[1]Institut de Physique de Rennes, Equipe Astrochimie Expérimentale, UMR 6251 du CNRS, Bâtiment 11c, Université de Rennes 1, Campus de Beaulieu, 35042 Rennes Cedex, France. [2]The University Chemical Laboratory, University of Cambridge, Lensfield Road, Cambridge CB2 1EW, UK.

*To whom correspondence should be addressed. E-mail: sebastien.le-picard@univ-rennes1.fr (S.D.L.); ian.sims@univ-rennes1.fr (I.R.S.); iwms2@cam.ac.uk (I.W.M.S.)